WORLD CONFERENCE ON TIMBER ENGINEERING 2025
BRISBANE, AUSTRALIA
Advancing Timber for the Future Built Environment

LATERAL TORSIONAL BUCKLING TESTS AND NUMERICAL SIMULATION OF GLUED LAMINATED TIMBER BEAMS

Vera Wilden[1], Benno Hoffmeister[2], Markus Feldmann[3]

ABSTRACT: The out-of-plane stability of slender timber beams under flexural bending is a key aspect of their structural design. The effects of lateral torsional buckling can be verified either using the equivalent member method or second-order theory with equivalent imperfections. As in some cases the results of the two approaches leads to different results, experimental investigations were performed to gain deeper insight of this phenomenon. This paper presents lateral torsional buckling tests on full scale glued laminated timber beams with material properties determined in detail.During fabrication of the glued laminated timber beams, the material properties of each timber lamella as well as the position of the lamellas in the beam were meticulously documented. The experimental sequence included assessment of bending and torsional stiffness, geometrical imperfection measurements, lateral torsional buckling tests and bending strength determination on glued laminated timber beams. The boundary and loading conditions were very close to the idealized assumptions. Based on the experimental results, numerical models were calibrated and validated.

KEYWORDS: Stability, Glued laminated timber, Lateral Torsional Buckling, Experimental Tests, Imperfections, Numerical Simulation

1 – INTRODUCTION

Glued laminated timber has emerged as the favoured option for long span girders, e.g. for gyms or warehouses. The common cross-sectional dimensions and materials provide sufficient resistance to flexural bending; however, large spans and slender cross-sections lead to increased member-slenderness and thus to a increased susceptibility to stability failure, in particular lateral torsional buckling (LTB). Eurocode 5 [1] offers provisions for the determination of the ultimate LTB resistance, either through the equivalent member method or by second-order analysis, considering effective geometrical initial imperfections. Since the above mentioned methodes sometimes lead to conflicting results, experimental tests were conducted for further investigating and deriving values for effective imperfections.This paper outlines a series of LTB-tests which, subsequently, were simulated numerically. The obtained experimental and numerical results are compared to current design rules.

2 – EXPERIMENTAL CAMPAIGN

Experimental tests are essential for understanding the stability behaviour of timber beams. Structural performance of slender glued laminated beams depends on various parameters, e.g. stiffness, imperfections, material strength and boundary conditions. The recording of all relevant properties and boundary conditions during implementation is necessary to derive validated values for design and numerical simulation. Followingly the state of the art regarding lateral torsional buckling test series found in literature is provided and afterwards the experimental tests conducted at RWTH Aachen University are described.

2.1 LATERAL TORISONAL BUCKLING TESTS IN LITERATURE

Key information from literature on LTB tests of timber beams with rectangular cross section are shown in Table 1. In total 69 of 222 lateral torsional tests were conducted with glued laminated timber beams [2,3,8,9].

Holley and Madsen [2] conducted in total 33 stability tests on eight girders under different load scenarios. The tests were stopped when the girder deflected laterally, before reaching the ultimate load. The investigation proved, that calculating the critical load assuming homogeneous material parameters led to results very close to the test outcomes. Brüninghoff [3] reported about three stability tests on slender rectangular beams through four point bending tests and confirmed Holley and Madsen's [2] findings.

Recent stability tests on glulam beams are described in [8,9]. Capellán [8] investigated the performance of glulam beams made of GL28h with a high relative slenderness using a three point bending test set up. Toepler et al. [9] focused on the load deformation behaviour of beams (GL24h) with small relative slenderness between 0,74 < $\lambda_{rel,m}$ < 1,04 under combined bending and compression. Three-point-bending test set-up with an eccentricity of 8 mm at top flange perpendicular to the beam axis was chosen. If a brittle member failure or the ultimate load was reached, the tests were terminated. Tensile failure due to bending, and shear and compression failure was observed.

[1] Vera Wilden, Institute of Steel Construction, RWTH Aachen University, Aachen, Germany, v.wilden@stb.rwth-aachen.de

[2] Benno Hoffmeister, Institute of Steel Construction, RWTH Aachen University, Aachen, Germany, hoff@stb.rwth-aachen.de

[3] Markus Feldmann, Institute of Steel Construction, RWTH Aachen University, Aachen, Germany, feldmann@stb.rwth-aachen.de

 https://doi.org/10.52202/080513-0140

Table 1: Experimental tests found in literature

Author/ Date of publication	strucutral system	No. tests	Exp. Aim
Hooley & Madsenal [2] 1964	3-P-bending cantilever	33	Critical Load
Brüninghoff [3] 1972	4-P-bending	3	Critical Load
Larsen & Theilgaard [4]1977	4-P-bending +compression	9	Effectives imperfections
Hindmann[5] 2005	Cantilever	120	Critical Load materials
Suryoatmono & Tjondro [6] 2008	3-P-bending	9	Performance & critical load
Xiao et al. [7] 2007	3-P-bending	13	Performance & ultimate load
Capellán [8] 2016	3-P-bending	14	Performance & ultimate load
Toepler [9] 2024	3-P-bending + compression	19	Performance & ultimate load

Only few published test results are suitable to validate buckling coefficients and initial imperfections related to the second-order behaviour. Except the tests in [8,9] which were conducted during the same period as the experiments at RWTH Aachen University, the tests were carried out on small-scale bending beams compared to today's standard dimensions. Furthermore, the test execution, measurement, evaluation and documentation of the results no longer correspond to the current state of the art.

2.2 LATERAL TORSIONAL BUCKLING TESTS AT RWTH AACHEN

Twelve LTB tests were conducted at RWTH Aachen in 2022 with main objective to investigate the load-deformation behaviour related to to geometrical and structural imperfections. To reduce the effect of structural imperfections the strength class of GL30h according to EN 14080 [10] was chosen for the specimens. The rectangular cross section dimensions were constant along the beam length (width ×depth=100 × 600 mm). Specimens with various relative slenderness ($\lambda_{rel,m}$) and spans L_s were included in the tests program. as illustrated in Table 2.

Table 2: experimental programme

Name	b/h [mm]	L_s [mm]	$\lambda_{rel,EC5*}$ [-]
K11/K12/K13	Gl30h 600 100	5500	1,04
K14/K15/K16		6500	1,10
K17/K18/K19		7500	1,16
K20/K21/K22		8500	1,20

b = width, h = depth, L_s = span, *calculated with characteristc material values, acc. to DIN EN 1995-1[1] DIN EN 1995-1 NA[11]

Manufacturing of the specimens

During the manufacturing process, the position of each lamella in girder was labeled. In combination with the data obtained from the grading process using the Golden Eye [12] grading machine, it was ensured that the material parameters at every position in the beam were known. Figure 1 shows the distribution plot of the measured dynamic elasticity modulus and estimated tensile strength of the individual lamella (in total 371 lamellas) and in Figure 2 a labelled beam is expemparily outlined. The estimated tensile strength refered to the position of the largest knot, which equals to the weakest point in the lamella. Remarkable is the wide range of the estimated strength (30 - 64 N/mm²) in combination with high elasticity moduli. The majority of strength values of the test specimens is above the 5% quantal minimum strength of 30 N/mm².

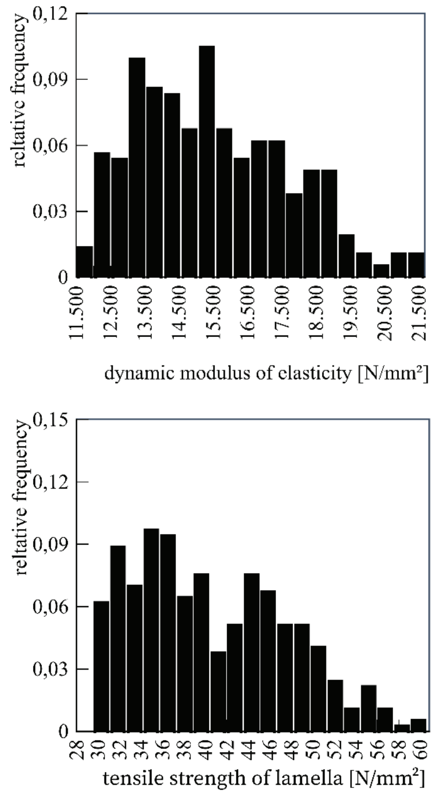

a) b)

Figure 1: a) b) grading parameters machined controlled using Golden Eye [12]

Figure 2: documentation of lamella position during manufacturing process

Stiffness Determination and strength parameters

To analyse values for effective geometrical imperfections and validate the numerical model, knowledge about the elastic stiffness for edgewise ($E_{y,exp}I_y$) and flatwise ($E_{z,exp}I_z$) bending as well as the torsional stiffness of the beam are required. Before conducting the LTB tests, the determination of flatwise bending and torsional stiffness ($G_{exp}I_T$) was performed using 3-point bending tests and torsional tests in the elastic range. For the above mentioned tests identical boundary conditions were applied. The edgewise elastic stiffness was derived from the load deformation curves of the LTB-tests.

The results of all parameters are summarized in Table 3. Prior to the stability test, the global and local geometric imperfections were measured using a tachymeter. Following the stability tests, the effectively undamaged members were tested in pure bending (4-Point-Bending-Tests) until reaching the ultimate moment resistance of the cross-section. To prevent shear failure during 4-Point-Bending tests, the beams with lengths of 5.5 m and 6.5 m were reinforced with self-tapping screws. Detailed information regarding stiffness and imperfection measurements are given in [13,14].

Lateral torsional buckling tests

A 3-point-bending test setup was chosen for the lateral torsional buckling test. The tests were performed in an innovative, newly developed testing rig, that enabled very precise control of loading and boundary conditions. A hydraulic jack was utilized to introduce the vertical load F_z, while a servo-controller ensured that the load direction remained vertical by following the lateral deformation of the beam without lateral constraints. Due to the horizontal control mechanism, very low lateral forces (F_y) were measured during the LTB-Test, Table 3. These low-level loads have no influence on the load-deformation-curves.

The vertical load was applied at the upper edge. In order to enable free torsion around the longitudinal-axis of the beam, a semi-spherical attachment was placed at the tip of the hydraulic jack. The distance between top edge of the beam and the contact point is a = 37.5 mm (for test K11/12, a = 42.5 mm). To prevent compression failure perpendicular to the grain, the load was introduced using a load distribution plate. The deformation-controlled tests with a rate of 0.05mm/s allowed for the identification of the ultimate limit state (governed by elastic stability) and the corresponding deformations. The tests were terminated when a significant cross-sectional deformation (several cm) occurred including a plateau of load-deformation curve or when the load exceeded a peak.

The instrumentation scheme consisted of 22 sensors to record the load-deformation behaviour, both in-plane and out-of-plane, at five points along the girder.

Results

For all tests, the specimens exhibited lateral deflection, and twisting around the longitudinal axis. As the geometrical length of the girder increased, a tendency of earlier lateral deflection was observed at stress levels significant below the strength. Representative load-deformation curves of four test specimens with different geometrical length are illustrated in Figure 3. In one specimen (K-11), during LTB test shear failure occurred. A longitudinal crack at one support area has developed. No further bending test was conducted for this specimen. The load-deformation curves of specimens K15 and K19 reached a significantly higher (maximum) load than the calculated critical load ($F_{max} \gg F_{cr}$), followed by sudden large lateral deformation and rotation around the longitudinal axis. A possible explanation follows from the measured initial geometric imperfection, as the initial rotation and lateral deformation were measured in oposite direction. The results of experimental tests are summarized in Table 3.

Figure 4 illustrates the comparison between the reduction curves according to DIN EN 1995-1-1[1] and prEN1995-1 [15] and experimental data. The diagram on the left (a) includes experimental data for relative slenderness and reduction factor, which are calculated with the measured-stiffness and strength values from experimental tests (equations 1-3). Due to different duration of LTB- and bending strength tests, the strength values were fitted in accordance with the investigation of Madison [16], see table 3.

$$\lambda_{rel,m} = \sqrt{\frac{M_{y,R}}{M_{cr}}} \tag{1}$$

$$k_m = \frac{maxM_y}{M_{y,R}} = \frac{maxF_z \cdot L_s}{4 \cdot f_{m,exp,red,madison} \cdot W_y} \tag{2}$$

$$M_{cr} = \frac{\pi}{l_{ef}} \cdot \sqrt{E_{mean,exp} I_z G_{exp} I_T} \tag{3}$$

Data points, which are above the Euler curves belong to test specimen K15 and K19, which reached significant higher loads than the critical load. Due to the fact, that relative slenderness and the reduction factor are influenced by the modulus of elasticity and shear, the beams K17, K18 with geometrical length of Ls= 7,5m indicated a higher relative slenderness than the beams K20-K22 with a longer geometrical length L_s= 8,5m. This effect is related to inherent material properties. For larger slenderness the experimental test results were below the reduction curve of DIN EN 1995-1-1 [1]. A comparison between tests and prEN1995 [15] illustrates that all test results lie above this continuous curve.

In Figure 3 the relative slenderness and reduction factor are calculated using stiffness and resistance based on the nominal characteristic values, according to DIN EN 14080. The reduction factor is above the curves of DIN EN 1995-1 [1] and prEN 1995 [15]. It is noteworthy that all values lie above or on the Euler curves.

https://doi.org/10.52202/080513-0140

Table 3: Test results

No	$f_{m,exp,madison}$ [N/mm²]	G_{exp} [N/mm²]	$G_{FEM,fit}$ ****) [N/mm²]	$E_{z,exp}$ [N/mm²]	$E_{z,FEM}$ [N/mm²]	$E_{y,exp}$ [N/mm²]	$E_{y,FEM}$ [N/mm²]	$maxF_z$ [kN]	$F_y(maxF_z)$ *****) [N]	$\lambda_{rel,m}$ (exp) [-]	$\lambda_{rel,m}$ EC5 [-]	k_m (exp) [-]
K11	-*)	751	680	13852	13621	13695	13621	127.7	-69.3	-		-
K12	42.0	784	686	15165	14782	13258	13603	130.4	-60.5	1.170	1.04	0.71
K13	34.5	787	713	11960	12417	11563	11503	131.1	-33.8	1.092		0.87
K14	36.8	764	723	13676	13769	13434	13182	92.9	-33.6	1.178		0.68
K15	28.1**)	723	708	12611	12575	12275	12301	100.4	74.7	1.064	1.10	0.96
K16	33.3	736	681	13150	12958	13104	13138	90.3	76.0	1.162		0.73
K17	43.7	775	722	15644	14144	13694	13681	75.4	64.6	1.331		0.54
K18	43.8	749	673	13296	12763	12890	12584	70.0	60.2	1.376	1.16	0.50
K19	35.2***)	740	671	13099	12903	12919	12960	96.1	58.9	1.241		0.85
K20	37.1	743	688	13730	14061	14090	14122	57.5	-16.6	1.318		0.55
K21	37.4	774	712	15262	14327	13882	14133	58.3	-12.4	1.297	1.22	0.55
K22	34.5	684	646	13757	13329	13208	13213	55.1	-12.2	1.312		0.57

*) shear failure during LTB tests
**) shear failure during bending strength test
***) shear failure first, than failure in tension zone
****) reduced shear modulus in FEM
*****) Measured lateral load F_y [N] due to lateral control system at the time of reaching the ultimate load $maxF_z$

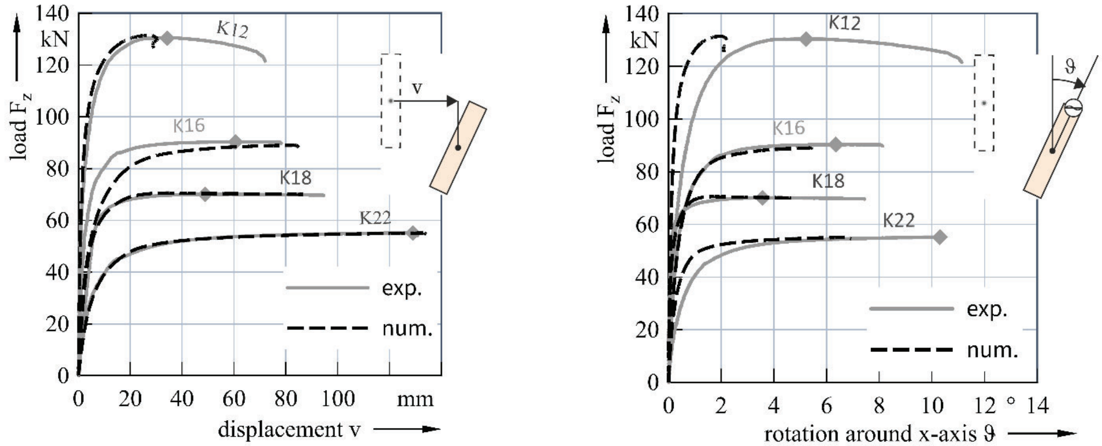

Figure 3: load deformation curves of the beam axis at midspan of K12/K16/K18/K22 and numerical recalculation for model validation

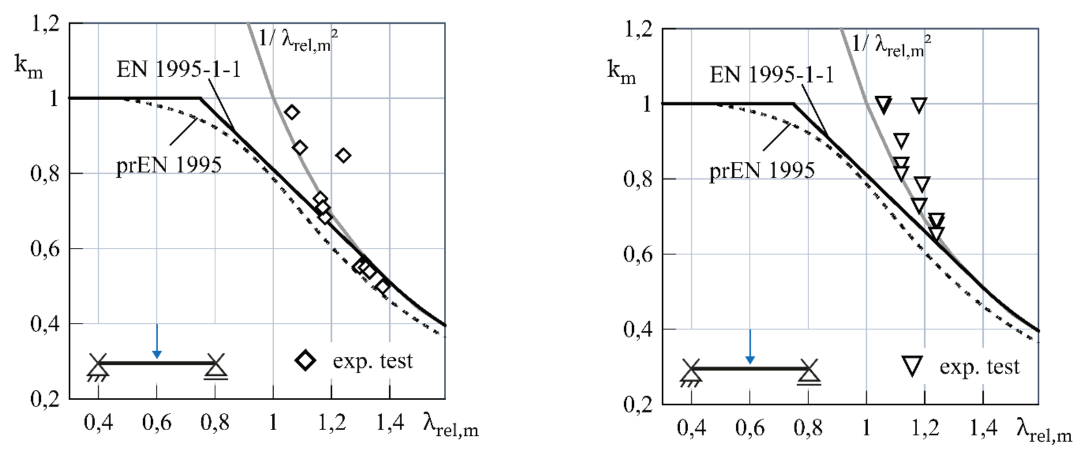

a) b)

Figure 4: Comparison between reduction curves and test results calculated with a) measured bending strength fm,exp and measured modulus of elasticity E=Mean($E_{z,exp}$; $E_{y,exp}$) and shear modulus from torsionaltest (G_{exp}) and b) with charakteristic values of bending strength, modulus of elasticity and shear modulus according to DIN EN 14080 [10]

https://doi.org/10.52202/080513-0140

3 –NUMERICAL SIMULATIONS

3.1 Lateral Torsional Buckling tests

The main objective of the numerical simulation was to validate the model based on the experimental results and expand the test matrix to investigate the influence of geometrical and structural imperfections on the performance of slender glulam beams.

The numerical simulations were conducted using the finite element software ABAQUS (version 2014) from Simulia. Hexagonal solid elements (C3D8) were employed for the modeling. After a mesh convergence analysis a mesh size of at least six elements across the width and 30 elements along the beam depth was found to be efficient. A detailed description of the model is given in Wilden [13].

Glued laminated timber is simulated in a parameterized numerical model using orthotropic material properties that represent the transverse anisotropy. To consider a non-linear material model, which includes pure plasticity under comperession parallel to the grain and brittle failure for tension parallel to the grain and shear, the user defined material model using the UMAT Subroutine in [17] was implemented. A maximum stress criterion is defined for each type of failure. If the threshold is exceeded, damage occurs. The elements of the stiffness matrix and maximum stress criterion must be provided individually; the selected input parameters are given in table 4.

Table 4: material parameter for numerical model

lamella section			
parameters		calculation	unit
stiffness	E_{11}	MP_{MOE}	N/mm²
	$E_{22} = E_{33}$	$E_{11}/30$	N/mm²
	$G_{12} = G_{13}$	$E_{11}/16$*)	N/mm²
	G_{23}	G13/13.8	N/mm²
poisson's ratio	$\nu_{12} = \nu_{13}$	0,501	-
	$\nu_{23} = \nu_{32}$	0,203	-
	$\nu_{21} = \nu_{31}$	0,011	-
Non linear material parameters			
strength	$f_{t,0,i}$	MP_{MOR}	N/mm²
	$f_{c,0,i}$	$5{,}5 \cdot f_{t,0,i}^{0,5}$	N/mm²
	$f_{t,90}$	0,4	N/mm²
	$f_{c,90}$	$0{,}007 \cdot \rho_k$ *)	N/mm²
	f_v	4,0	N/mm²
	f_{roll}	0,5	N/mm²
fracture Energy	$G_{f,t,0}$	6,0	N/mm
	$G_{f,t,90}$	0,5	N/mm
	$G_{f,v}$	1,2	N/mm
	$G_{f,roll}$	0,6	N/mm
fictitious viscous	η	0,0001	N/mm

*) adapted during validation process
MP_{MOE} = **M**aterial **P**roperty **M**odulus **O**f **E**lasticity
MP_{MOR}= **M**aterial **P**roperty **M**odulus **O**f **R**upture

Structural imperfections

By combining the grading data of each lamella with information about their positions in the girder, a digital twin of each specimen is generated. The material parameters are constant across the lamellas width, while the material properties in longitudinal direction of the lamellas vary. The outcome of a sensitivity analysis indicated an interval length of 25 mm for the implementation of different material properties along the length of the lamella. In particular, the knot parameter can be modelled with sufficient accuracy. A finger joint is arranged between two lamellas and implemented in the numerical model, using the recommendations for determing the material properties of Fink [18].

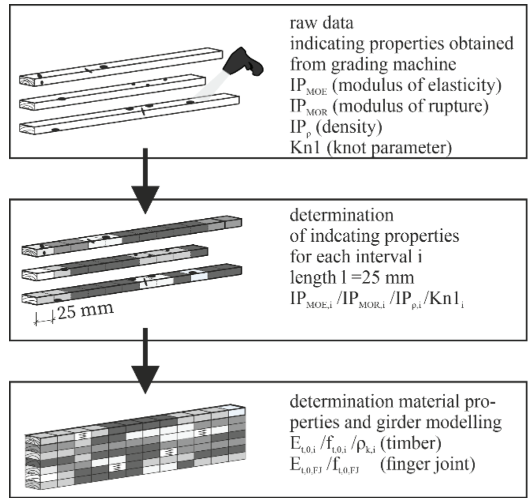

Figure 5: generation digital twin using python scripting

Boundary conditions and load application

The load introduction at the upper eadge in the centre of the span was modelled in detail with all steel components (load introduction plate, sphere, semi-spherical support shell). The unavoidable friction between the sphere and the support shell influences the rotation of the beam, which has a minor effect on the load-deformation behaviour. Consequently, the existing contact surfaces of the steel components were interconnected through contact relationships and assigned corresponding coefficients of friction perpendicular to the contact surface (steel-steel: μ=0.203; steel-timber: μ=0.5).

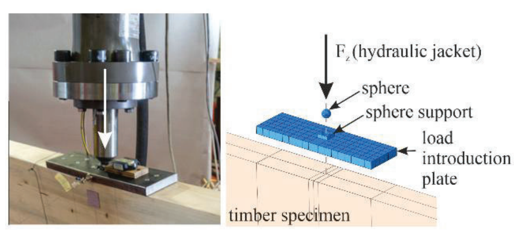

a) b)

Figure 6: load application a) test-set up b) numerical model

The lateral supports were close to idealized fork supports, with vertical line supports, which prevent lateral dsplacements (z-direction). In vertical direction (y-direction, Figure 7), the test specimen was placed on a load-distributing steel plate, which was part of a supporting frame and prevented vertical displacement and provided free rotation around the z-axis in geometrical cross-sectional axis of the test specimen. In the numerical model, a kinematic coupling jointed a surface at lower edge with the center of geometric cross section of the beam. The center point was fixed in y-direction. Due to numerical stress concentration, a hyper-elastic material model was used in the area of boundary conditions.

https://doi.org/10.52202/080513-0140

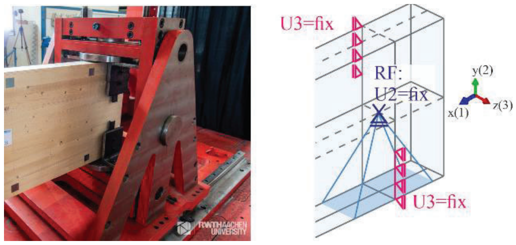

a) b)

Figure 7: support a) test-set up b) numerical model

Firstly the measured geometrical imperfection were introduced in the model, then an ultimate load analysis was conducted via a displacement-controlled load application and considering the measured lateral forces during simulation.

For the validation of the digital twins the experimentally recorded load-deformation-curves (lateral displacement and rotation around x-axis) were used. Figure 3 shows an example of the comparison for four tests. The results can be summarised as follows:

The caculction of the "shear moduls" in accordance to DIN EN 384 [19] and $G_{mean}= E_{0,mean}/16$ leads to an overestimation of the resistance in the simulations. By reducing the shear stiffness via the E/G ratio (generally $21<E/G<23$; for the shortest beams $25<EG<26$) the load-deformation curves were in good agreement. The comparison between the experimentally determined shear modulus (G_exp) and the mean shear modulus derived from the simulation indicates that the shear modulus in the simulation needs to be reduced by about 18%. Further research is necessary, to clearify whether the reduction of the shear modulus is due to time-dependent behavior [20,21,22] or due to a nonlinear load-deformation behavior of wood under torsional load [23,24].

An average modulus of elasticity around strong ($E_{y,\ FEM}$) and weak axis ($E_{z,\ FEM}$) can be determined from the load-deformation curves as result of the simulations of the flexural bending and LTB tests in analogy to the experimental tests. There is a very good agreement between the numerical and experimental moduli of elasticity, as it can be observed in Table 3.

If applying the minimum shear strength according to DIN EN 14080 [10] in the numerical analysis, the short span girders show shear failure at the area of the supports or next to the load application. Similar effects were not observed in the tests, and therefore higher values of shear strength values were considered for the numerical investigation. A literature review shows, that shear strength determined by published torsional tests is 9,3 N/mm² [23].

In the numerical model the compression strength perpendicular to the grain was increased, due to the activation of surrounding grains under compression perpendicular to the grain.

3.1 Bending tests

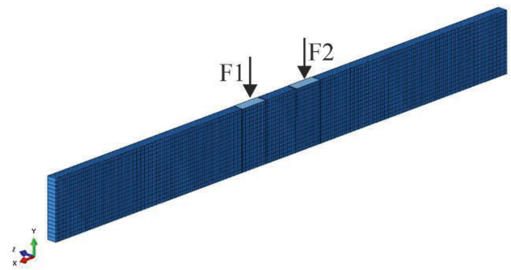

Figure 7: numerical model for determining bending strength

The bending strength was also determined numerically. To achieve bending failure in experimental tests, shear reinforcement using self-drilling screws was implemented in girders with shorter spans. To consider the reinforcement, the shear strength in the simulation was increased to $f_v = 9$ N/mm².

Depending on the length of the beam, the position of loads in the force-controlled four-point-bending test varied. Load and boundary conditions were implemented in an idealised manner using reference points and coupling conditions. In experimental tests, the deformation out of plane was prevented, so in numerical simulation non linear geometrical effects were excluded.

Load deformation behaviour

The measured load-displacement curves obtained during bending tests served to validate the numerical model. Figure 8 contains a comparison between the resulting loads (F1 and F2) - deformation curves at midspan of numerical models and experimental tests. In tests only the resulting load at hydraulic jacket was measured. The measured load was halved for the comparsion with numerical tests. Due to the variation of material parameters in the numerical model, the measured load F1 and F2 are slightly different. In general, the load deformation curves of the numerical model and experimental tests are in good accordance.

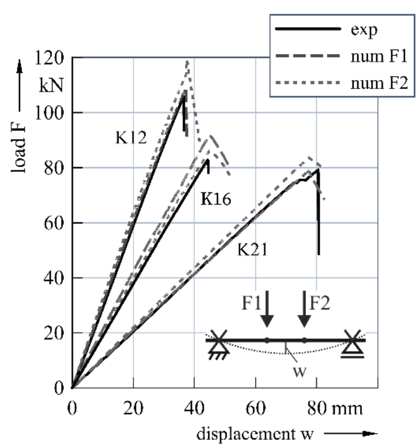

Figure 8: Bending test: Comparison of tests and numerical load-displacement curves for three specimens

The ultimate load obtained from experimental tests and numerical simulation enable a recalculation of bending strength. A comparison of experimental and numerical bending strength test results is shown in Figure 9. The values of bending strength derived from the numerical simulations are slightly overestimated (less than 7%). A more pronounced difference can be identified in test K18. However, the numerical result of K18 lies on the safe side.

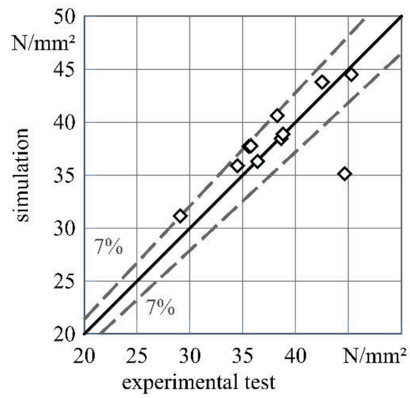

Figure 9: Bending test: Comparison of test and simulation results

Location of failure

A brittle failure mode was observed during 4-point-bending tests. The location of failure was determined by analysing video recordings of tests and was compared to numerical results, see Figure 10. Table 9 gives an overview of positions of failure during tests and simulations as well as the estimated tensile strength $f_{t,0}$ at location x. Furthermore it is noted, weather the location is a finger joint (FJ) or a knot area (KA). The simulation accurately predicted the failure position for 50% of the conducted tests. Failure location in the correct lamella was predicted in 30% of the tests. The estimated strengths are very close to each other. In two cases (K14, K18) the failure location and the estimated stress at the different locations were very close to each other. It should be noted that the determination of the exact location of the damage initiation in the tested beams was not always possible due to limited quality of the videos.

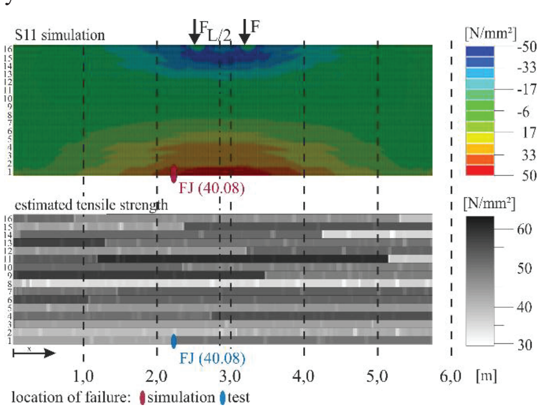

Figure 10: Comparison of failure location in test K12

Table 5: Position of failure

No	Number – position x of lamella *) [-]- [mm]		Interval		$f_{t,0}$ [N/mm²]	
	Exp.	Num.	Exp.	nu m.	exp.	num .
K12	1-2200	1-2200	FJ	FJ	40,1	40,1
K13	2-3375	2-2600	KA	FJ	33,3	31,3
K14	1-4100	1-2600	KA	KA	45,76	46,6
K16	1-3300	1-3300	FJ	FJ	36,9	36,9
K17	2-2750	2-4275	KA	KA	46.1	37,3
K18	1-4000	1-4250	KA	FJ	34,5	39,4
K19	1-490	1-4290	FJ	FJ	35,8	35,8
K20	1-5340	1-3465	FJ	KA	35,6	34,5
K21	1-3830	1-3165	FJ	KA	43,1	40,6
K22	1-3210	1-3432	FJ	KA	44,7	44,4

exp. = experimental test, num. = simualtion
KA = Knot areaAstbereich, FJ = Finger joint
*) position x, see figure 10

6 – CONCLUSION

The paper describes a thorough investigation of the stability of twelve slender glulam timber beams including an extended experimental campaign, numerical simulations and comparison with the current design provisions. Comparison of experimental test results with theoretical reductions curves indicates that the existing reduction curves considered in prEN 1995 [15] underestimate the performance of the glued laminated timber beams.

Validated FE models confirmed reliably the load-deformation and load-bearing capacity obtained from stability and bending strength tests. The models enabled a further numerical study to identify the influence of imperfection variables and other material properties on the global response of slender glued laminated timber beams.

7 – ACKNOWLEDGEMENT

The authors are grateful for providing of specimens by Poppensieker & Derix GmbH & Co and Mictrotec Srl Gmbh.

8 – REFERENCES

[1] “EN 1995-1-1: Eurocode 5: Design of timber structures - Part 1-1: General – Common rules and rules for buildings”; 2004.

[2] R. Hooley and Borg Madsenal. “Laterally stability of glued laminated beams.“ In: Journal of structural division (1964), pp. 201-218.

[3] H. Brüninghoff. “Spannungen und Stabilität bei quergestützen Brettschichtholzträgern.“, PhD thesis. Germany Karlsruhe: University Karlsruhe, 1977.

[4] H. J. Larsen, and E. Theilgaard. “Laterally loaded timber columns.“ In: Journal of structural division (1979), pp. 1347-1363.

[5] D. P. Hindmann, H. B. Manbeck and J. J. Janowiak. “Measurement and prediction of lateral torsional buckling loads of composite wood materials: rectangualr sections.“ In: Forest products journal 9 (2005), pp. 42-47.

[6] B. Suryoatmono and A. Tjondr. “Lateral-torsional buckling of orthotropic rectangular section beams.“ In: WCTE (2008), Japan.

https://doi.org/10.52202/080513-0140

[7] Q. Xiao. “Lateral Torsional Buckling of Wood Beams.” Master thesis. Ottawa, Canada: Departmene of Civil Enigineering, University of Ottawa, 2014.

[8] M. G. Capellán. “Estudio Teórico-experimental del pndeo lateral en vigas de madera laminada encolada.“ PhD thesis. Santander, University of Cantabria, spane, 2016.

[9] J. Töpler and U. Kuhlmann. “Lateral Torsional buckling of glulam beams.“ in Proceedings of the 10th meeting of International Network on Timber Engineering Research INTER, 2023.

[10] “DIN EN 14080 Timber structures – Glued laminated timber and glued solid timber – Requirements, 2013.

[11] DIN EN 1995-1/National Anex Germany. “Eurocode 5: bemessung und Konstruktion von Holzbauteilen, Teil 1-1: Allgemeines — Allgemeine Regeln und Regeln für den Hochbau“ , 2013.

[12] M. Bacher. “Comparison of different machine strength grading principles.” Cost Action E53 Conference, Delft, Netherlands, 2008.

[13] V. Wilden. “Beitrag zum Tragverhalten von schlanken Brettschichtholzbindern“ unpublished. PhD thesis, RWTH Aachen University, 2025.

[14] V.Wilden, B. Hoffmeister, and M. Feldmann. “Ein mechanisch konsistenter Ansatz fur den Stabilitatsnachweis fur Holztrager unter Druck und Biegung um die starke Achse – Teil 2 – Versuche und Numerik.” In: Bautechnik 101, Sonderheft Holzbau 2 (2024), pp. 53–63.

[15] prEN 1995-1-1 (draft version) “Eurocode 5: Design of timber structures – Common rules and rules for buildings – Part 1-1: General”, CEN/TC 250/SC 5 N 1615, September 2022.

[16] L. W. Wood. “relation of strength of wood to duration of load.“ USDA Forest service, Forest products laboratory, University of Wisconsin, 1960.

[17] C. Sandhaas. “Mechanical behaviour of timber joints with slotted – in stell plates.”, PhD thesis. Delft, Technische Universität Delft, 2012.

[18] G. Fink. “Influence of varying material properties on the load-bearing capacity of glued lamianted timber.”, PhD thesis. Zürich: ETH Zürich, 2014.

[19]“DIN EN 384 Structural timber – Determination of characteristic values of mechanical properites and density”, 2022

[20] G. Schaar. “Beitrag zur Torsionselastizität von Hölzern in Abhängigkeit von der Holztemperatur und der Belastungszeit.“ In: Holz als Roh und Werkstoff, pp. 57-60, 1986.

[21] K. Möhler and K. Hemmer. “Verformungs- und Festigkeitsverhalten von Nadelvoll- und Brettschichtholz bei Torsionsbeanspruchung.“ In: Holz als Roh und Werkstoff. pp. 473-478, 1977.

[22] H. Benning. “Beitrag zur Traglastberechnung stabilitätsgefährdeter Brettschichtholzträger.“ PhD thesis, Ruhr-University Bochum, 1997.

[23] M. Khokhar. “The evaluation of shear properties of timber beams using torsion test method.”, Edinburgh, Schottland: Einburgh Napier University, 2011.

[24] R. Gupta and T. Siller. “Shear Strength of Structural Composite Lumber Using Torsional Tests.“ In: Journal of Testing an Evaluation, Vol 33 No. 2 , pp. 110-117, 2005.